Journal of Electron Spectroscopy and Related Phenomena 195 (2014) 332–336

Contents lists available at ScienceDirect

Journal of Electron Spectroscopy and Related Phenomena

journal homepage: www.elsevier.com/locate/elspec

# Coulomb imaging of the concerted and stepwise break up processes of OCS ions in intense femtosecond laser radiation

Benji Wales[a], Éric Bisson[b], Reza Karimi[a], Samuel Beaulieu[b], Ali Ramadhan[a], Mathieu Giguère[b], ZiJian Long[a], Wing-Ki Liu[a], Jean-Claude Kieffer[b], François Légaré[b], Joseph Sanderson[a,*]

[a] Department of Physics and Astronomy University of Waterloo, 200 University Avenue West, Waterloo, ON N2L 3G1, Canada
[b] Institut National de la Recherche Scientifique, Centre Énergie Matériaux Télécommunications, Varennes, QC J3X 1S2, Canada

ARTICLE INFO

*Article history:*
Available online 14 May 2014

*Keywords:*
Coulomb imaging
Molecular geometry
Concerted break up
Stepwise break up
Femtosecond laser
Molecular deformation

ABSTRACT

We study the break up of OCS in intense femtosecond laser radiation using the FEMPULS technique to vary the laser pulse duration from 7 fs to 200 fs. Newton and Dalitz plots show the progression of molecular deformation and break up for $OCS^{3+}$ and $OCS^{4+}$. For increasing pulse length, the concerted three body dissociation exhibits increasing bending, and the amount of stepwise dissociation decreases. For the longest pulses however the stepwise process increases again. Both phenomena can be interpreted in terms of the effect of the laser field on lower charge states and the behaviour of a wave packet on a saddle point potential. The experiment illustrates the ability of the Coulomb imaging method to track molecular geometry and dynamics and indicates a new path to laser control of molecular parameters.



## 1. Introduction

Intense femtosecond (fs) lasers are ideal tools for imaging molecular structure and dynamics, and have been used for more than twenty years initially through uncorrelated methods such as momentum imaging [1–4] but more latterly through the powerful coincidence method of Coulomb Explosion Imaging (CEI) [5–7], in particularly since the advent of hollow fibre compressors the equilibrium structure of molecules has been within reach [8–13]. More recently methods such as electron ion coincidence [14] and high harmonic tomography have also shown promise [15–18]. Theoretical advances have identified the origin of phenomena observed experimentally such as charge resonance enhanced ionisation (CREI) [19] and laser induced dynamics [20].

We have recently made an experimental advance [12,13] by varying the pulse duration from few cycles (<10 fs) to 100 s of fs and making a series of careful measurements of fragmentation. Crucially we maintain a nearly constant ratio of final dissociation products from triply and doubly charged molecular ions which ensures we are exploring the same break up processes for each pulse duration. This has revealed aspects of laser–molecule interaction not visible in earlier work which used a fixed pulse duration [1–11]. This improvement is analogous to the increase in information retrieved about dynamics from a movie compared to a single snapshot. The new multidimensional approach is referred to as FEmtosecond Multi-PUlse Length Spectroscopy (FEMPULS) and has enabled us to make significant advances in the understanding of dynamics and ionisation dynamics in triatomic molecules. Firstly in the case of $CO_2$ [12], by monitoring the total kinetic energy released (KER) of the observed dissociation channels from 3+ to 6+ using the 3D-ion-momentum coincidence method [5], we were able to show that the KER from fragmentation on the 3+ charge state is nearly constant with pulse duration even for few cycle pulses. When we compare the KER with a simulation of the Coulomb explosion (CE) assuming point-like ions, we found that the measured energy release is around 70% of the Coulombic energy. This contrasted with the higher channels such as 6+ (2,2,2) which exhibited low energy release of close to 50% for long pulses, and high energy release up to 90% for short 7 fs pulses. The pattern not only revealed that the 3+ state is never Coulombic but also pinpointed it as the state from which CREI to higher charge states is initiated. In addition, by monitoring the individual energy released by the respective fragment ions, we showed that there was a progression in the deformation of molecular structure with pulse duration. In the case of $N_2O$ [13] we focused on the low molecular charge 3+ and 4+ and were able to observe a new break up channel for the shortest pulses (sub 7 fs) in which a metastable $N_2^{2+}$ ion is generated, $N_2O^{3+} \rightarrow N_2^{2+} + O^+ \rightarrow N^+ + N^+ + O^+$ as well as a new stepwise

* Corresponding author. Tel.: +1 519 885 1211x36109.
*E-mail address:* j3sander@uwaterloo.ca (J. Sanderson).

http://dx.doi.org/10.1016/j.elspec.2014.05.003
0368-2048/

channel for 4+, $N_2O^{4+} \rightarrow N^{2+} + NO^{2+} \rightarrow N^{2+} + N^+ + O^+$. Crucially we used the Dalitz plotting method [21] to express the structure of the molecule for different lengths of exposure to the intense laser radiation, and were able to effectively deduce aspects of stretching and bending.

Here we use the FEMPULS method, along with both Dalitz and Newton plots, to determine the changes in structure and break up processes for OCS in femtosecond laser pulses varying in pulse length from less than 7 fs to 200 fs. OCS structure and break up has been studied previously using femtosecond laser interaction [22–24] or highly charged ion impact [24–26] but here we expect to be able to reveal new aspects of processes such as metastable break up channels $OCS^{3+} \rightarrow CO^{2+} + S^+ \rightarrow O^+ + C^+ + S^+$, and how they change with pulse length.

## 2. Experimental

The experiments were performed at the Advanced Laser Light Source using the multi-kHz titanium–sapphire (Ti–Sa) laser system (KMLabs Dragon laser system; 5 kHz, 5 mJ, 35 fs pulse duration). Few-cycle pulses (7 fs) are obtained using nonlinear propagation in a hollow core fibre filled with Ar and by dispersion compensation using chirped mirrors. To achieve longer pulse duration, the fibre was evacuated. Using an acousto-optic programmable dispersive filter located in the stretcher of the Ti–Sa amplifier, we applied second order dispersion ($\Phi^{(2)}(fs^2)$) to achieve the desired pulse duration. As in [12,13] we maintain the appearance of our TOF spectrum by adjusting the peak laser power so that the relative amounts of final triply and doubly charged fragment ions stays constant. Because enhanced ionisation becomes more important for longer pulses, this results in intensities which vary between $3 \times 10^{15}$ for 7 fs pulses and $2 \times 10^{14}$ W cm$^{-2}$ at 500 fs. The laser pulses are focused by a parabolic mirror ($f$ = 10 cm) on a well-collimated supersonic jet of OCS inside a uniform-electric-field ion imaging spectrometer. The fragments are detected and their full 3D momenta are determined using a time- and position-sensitive delay-line anode detector at the end of the spectrometer (RoentDek Handels GmbH). The atomic and molecular fragment ions were measured in double or triple coincidence: $CO^{a+} + S^{b+}$ and $O^{a+} + CS^{b+}$ or $O^{p+}$, $C^{q+}$ and $S^{r+}$ ($a + b = 2$ or 3, $p + q + r = 3$ or 4). Ions are identified as the result of the fragmentation of a single molecule only if their total momentum is close to zero ($< 5 \times 10^{-23}$ kg m/s), using this criteria we can distinguish between the degenerate $S^+$ and $O^{2+}$ ions as well as discriminate against ions resulting from more than one molecule [27].

## 3. Results

One feature which emerges from the coincidence search for modes of molecular ion break up for OCS at a pulse length of 7 fs is the strong signal from binary dissociation channels which include doubly charged molecular ions $OCS^{3+}$ and $OCS^{4+}$, $CO^{2+} + S^{2+}$ and $O^{2+} + CS^{2+}$ are both present in addition to $CO^{2+} + S^+$ and $O^+ + CS^{2+}$ previously observed in highly charged ion collision [25,26]. Although it is a new observation for laser induced dissociative ionisation the existence of channels which involve these species is not necessarily surprising as the nuclear interaction potential for the triply charged state [28] as with $CO_2$ [20] is expected to be a saddle point in which expansion of one bond is the energetically favourable dissociation path. To confirm the form of the potential for $OCS^{3+}$ we measure the kinetic energy release distribution of the (1,1,1) channel. Fig. 1a shows that the distribution for (1,1,1) [29] is largely unaffected by pulse length up to 100 fs and peaks at around 64% of the expected Coulombic value. Since, for the shortest pulses, we expect that the molecule will be ionised before the bonds have a chance to expand, this is a strong indicator that the 3+ potential is not Coulombic near to equilibrium and in fact has a shallow minimum or 'quasi bound' region which stretches out to a local maximum. The position of this maximum can be estimated from the ratio of energy released to the expected Coulombic value, $E/E_{\text{Coulombic}} = 0.64$ indicates that at around $1.56R_{\text{eqilibrium}}$ there is a maximum after which the potential becomes Coulombic. This is in good agreement with calculations of low lying potentials in $OCS^{3+}$ [28]. Only for pulses of 200 fs and higher, do the bonds stretch to the Coulombic region, where energy begins to decrease with pulse length. By contrast the (1,1,2) channel shows significant decrease in energy for all increases in pulse length, until the critical distance for enhanced ionisation is reached. It appears from this that the $OCS^{4+}$ potential is purely repulsive when both bonds break. We will return to this later.

In order to categorise the possible break up channels for the 3+ and 4+ channels we use the Dalitz plot method, a well established technique for displaying the possible molecular dissociation geometries in a two dimensional histogram [21]. The plot is typically used for symmetrical molecules but functions in a similar fashion for the asymmetric OCS molecule where the total geometrical phase space is represented by a diagonal oval. The histogram is simply generated by plotting the fraction of energy carried by the carbon ion along the $y$-axis while the difference in the fraction of energy between the sulfur and oxygen ions is plotted along the $x$-axis. The resulting space is a well defined oval where each point represents specific arrangements of momentum vectors (Fig. 2a). Though the geometry of the molecule and the momentum vectors are related in a nontrivial way, a simple simulation shows that the equilibrium geometry should appear on the Dalitz plot at (0.11,−0.29).

Bending of the molecule in a concerted dissociation process results in a reduced angle between the outside momentum vectors and is associated with approximately vertical changes from the equilibrium point on the Dalitz plot. This is indicated by a black oval shown in Fig. 2b which shows the (1,1,1) channel for a 7 fs pulse. Points further separated horizontally from the main distribution represent increasing amounts of asymmetry in bond length and are indicative of asynchronous break up. Fragmentation of OCS into a metastable CO ion appears as a diagonal indicated by the dashed red ovals in Fig. 2b while a break up which involves a metastable CS ion appears as data along a diagonal indicated by the dashed yellow ovals. The uniform density of the diagonals indicates the molecular fragment behaves as a rigid rotor spinning away from the remaining atomic ion [6,30]. It is worth noting that both of these processes are strong in the case of OCS and are represented on a linear intensity scale, whereas for the $CO_2$ and $CS_2$ molecules [6,30] the stepwise process needed to be shown on log plots. To further examine the stepwise processes we use normalised Newton plots [30] of the (1,1,1) channel at 7 fs firstly with the $O^+$ ion as the frame of reference and secondly with $S^+$. Fig. 3a shows the momentum of the $C^+$ and $S^+$ ions relative to $O^+$ with the concerted channel represented by two intense islands, and the stepwise channel $CS^{2+} + O^+$ represented by two diffuse half rings (which are offset from each other), a more faint feature consisting of horizontal jets is explained by plotting momentum relative to the sulphur ion, in Fig. 3b here a similar picture emerges but the diffuse ring now represents the $CO^{2+} + S^+$ channel and consists of the data points which were present in the jets of Fig. 3a. Fig. 3c shows the Newton plot for the (1,1,2) channel relative to $S^{2+}$ again showing a diffuse ring which represents $CO^{2+} + S^{2+}$, in this case there are no faint jets because there is no alternative stepwise channel. One feature of these rings is their uniformity, which indicates the stability of the molecular ion, such that it can perform many rotations before dissociating. Estimates for $CO^{2+}$ and $CS^{2+}$ have ranged from 100 fs [30] to picoseconds [6].

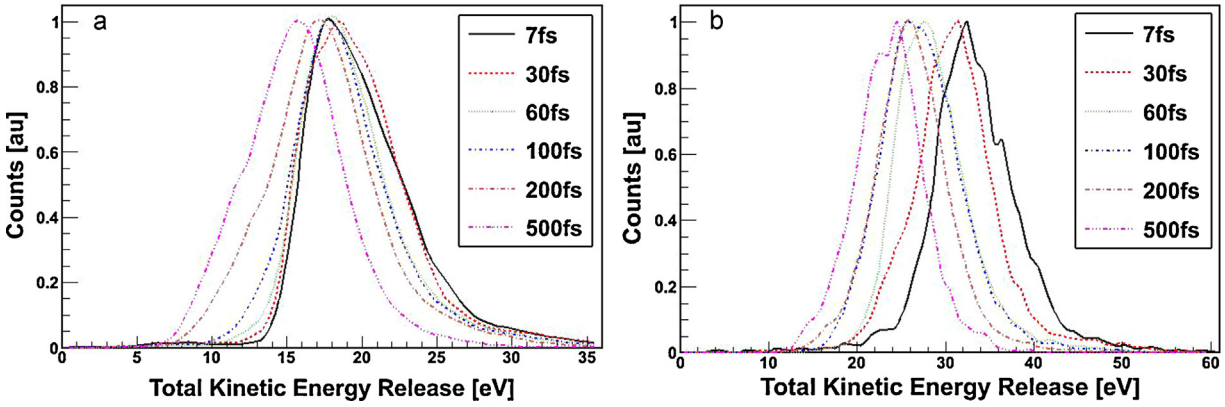


**Fig. 1.** Total kinetic energy release distributions for (a) the (1,1,1) channel and (b) the (1,1,2) channel of OCS, showing that the peak value does not depend on the pulse length for (1,1,1) below 200 fs and by contrast, for (1,1,2), the peak value systematically decreases with increasing pulse length.

Fig. 4 shows the Dalitz plots from 7 to 200 fs, normalised so that the peak signal is always the same colour, revealing morphological differences as a function of pulse length. These Dalitz plots indicate the progression of the molecular wave packet on the 3+ and 4+ states, for short pulses the geometries are close to equilibrium for the concerted channel. As the pulse gets longer the concerted process spreads out along the vertical bending axis indicating that the laser induced bending process proposed for $CO_2^{6+}$ [12] also exists for OCS. As in $CO_2$, it is the potentials of lower charge states in the laser field where the molecular bending takes place, before it reaches 3+ and 4+. We can also see that the central region of the Dalitz plot (indicated by the black oval in Fig. 2b), showing the concerted process, becomes wider with pulse length (in the $x$ dimension) and that for longer pulses the region becomes wider at the top than the bottom of the plot. Points on the Dalitz plot to the left or right of $x = 0.11$ indicate less concerted or progressively asynchronous bond breaking while points above $y = -0.29$ indicate more bending. The trend indicates that as the pulse length increases, molecules bend more and bonds break more asynchronously. This is not clear from the energy release of Fig. 1, which seems to indicate that bonds are not changing below 200 fs because energy release is not decreasing. In fact bonds are almost certainly stretching as they bend as observed for higher channels [12] but the stretch must be in a region of the potential which is relatively flat and so does not lead to decreased kinetic energy release. The effect of pulse length can be revealed more precisely in the Dalitz plot if they are normalised to have the same total number of counts, then the peak channels do not have the same number of counts from one plot to the next but the plots effectively represent the spreading of the final state wave packet, Fig. 5 shows such a normalised plot for the

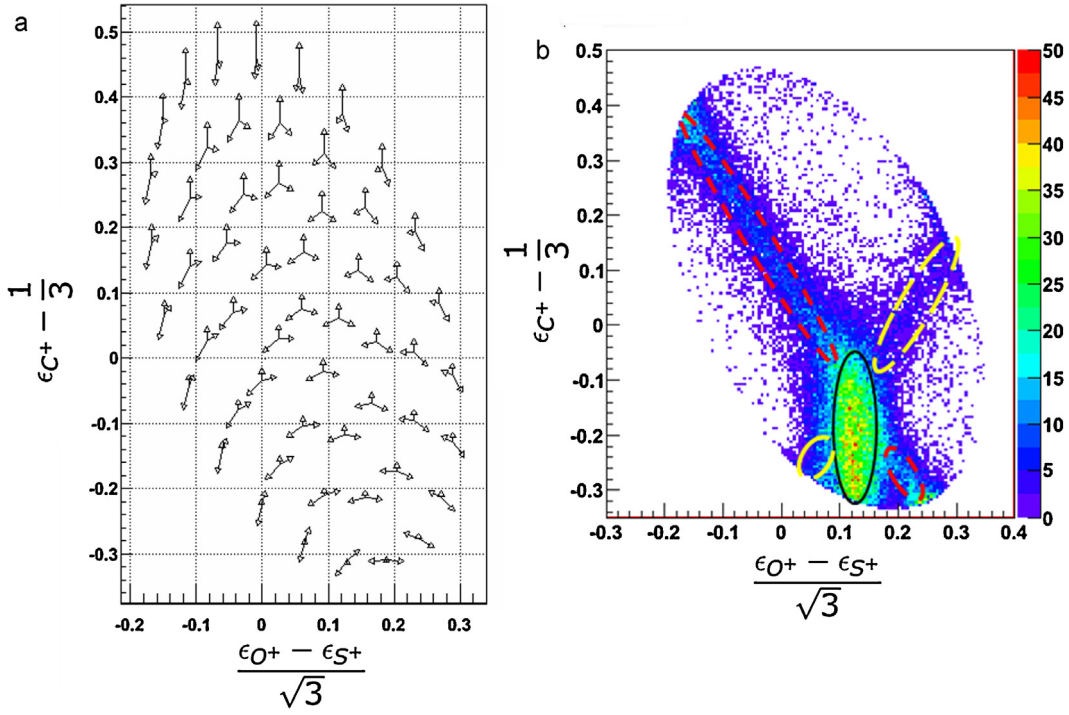


**Fig. 2.** Dalitz plot for the (1,1,1) channel of OCS at 7 fs. The $x$ axis indicates the difference between the fraction of total energy release (epsilon) by the O and S ions and the $y$ axis is fraction of energy release of the C ion. (a) The relationship between the points on the plot to the momentum vectors of the three fragments, the C is vertical, S to the left and O to the right. (b) Experimental data, the black oval indicates the concerted processes (increase in $y$ indicates bending), the dashed red ovals indicate a stepwise process in which the CS bond breaks first, $OCS^{3+} \rightarrow CO^{2+} + S^+ \rightarrow C^+ + O^+ + S^+$ and the dashed yellow ovals represent a stepwise process in which the CO bond breaks first, $OCS^{3+} \rightarrow CS^{2+} + O^+ \rightarrow C^+ + O^+ + S^+$. (For interpretation of the references to color in this figure legend, the reader is referred to the web version of this article.)

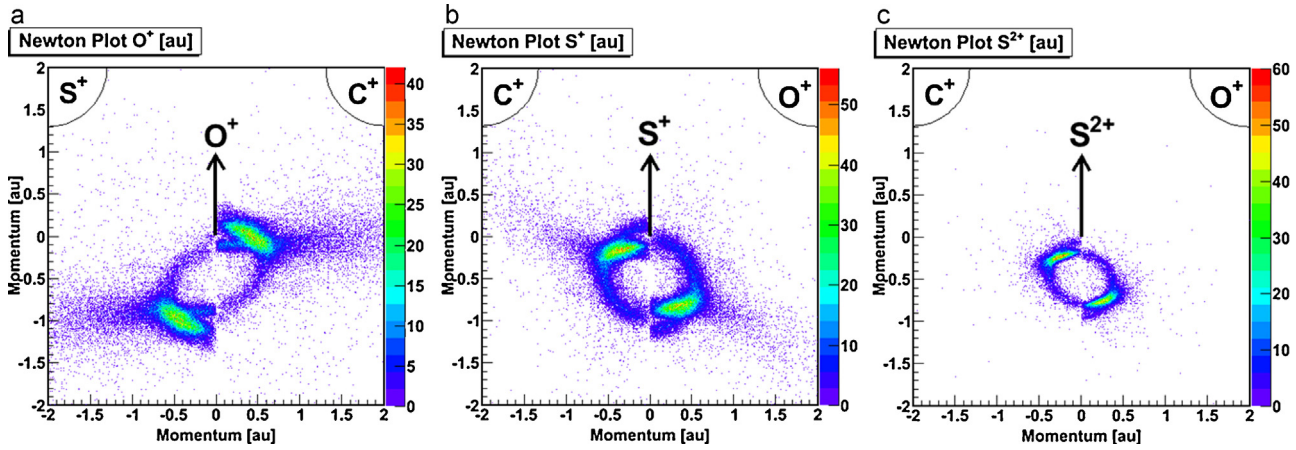


**Fig. 3.** Newton plots of (1,1,1) and (1,1,2) recorded at 7 fs. (a) Plot in which the $O^+$ ion momentum has been normalised to 1 as indicated by the arrow, $S^+$ momentum to the left and $C^+$ to the right. The ring structures represent the stepwise process $OCS^{3+} \rightarrow CS^{2+} + O^+ \rightarrow C^+ + O^+ + S^+$. (b) Plot in which the $S^+$ ion momentum has been normalised to 1 as indicated by the arrow, $C^+$ momentum to the left and $O^+$ to the right. The ring structures represent the stepwise process $OCS^{3+} \rightarrow CO^{2+} + S^+ \rightarrow C^+ + O^+ + S^+$. (c) Plot in which the $S^{2+}$ ion momentum has been normalised to 1 as indicated by the arrow, $C^+$ momentum to the left and $O^+$ to the right. The ring structure indicates the stepwise process $OCS^{4+} \rightarrow CO^{2+} + S^{2+} \rightarrow C^+ + O^+ + S^{2+}$. In all plots the bright green oval areas are from the concerted process and the diffuse region projecting from the rings represent the alternate stepwise process, not present for $OCS^{4+}$. (For interpretation of the references to color in this figure legend, the reader is referred to the web version of this article.)

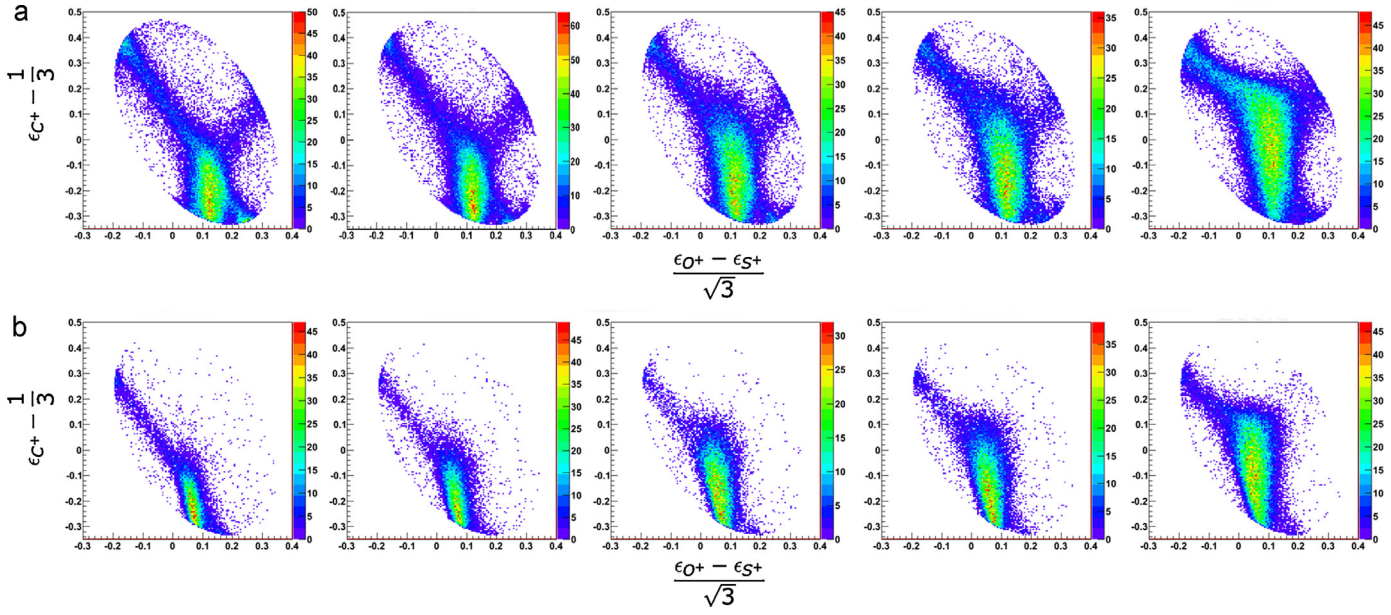


**Fig. 4.** (a) Dalitz plot of (1,1,1) channel from 7 to 200 fs (left to right 7, 30, 60, 100 and 200 fs) showing the vertical lengthening and widening of the concerted process. (b) Similar process for (1,1,2).

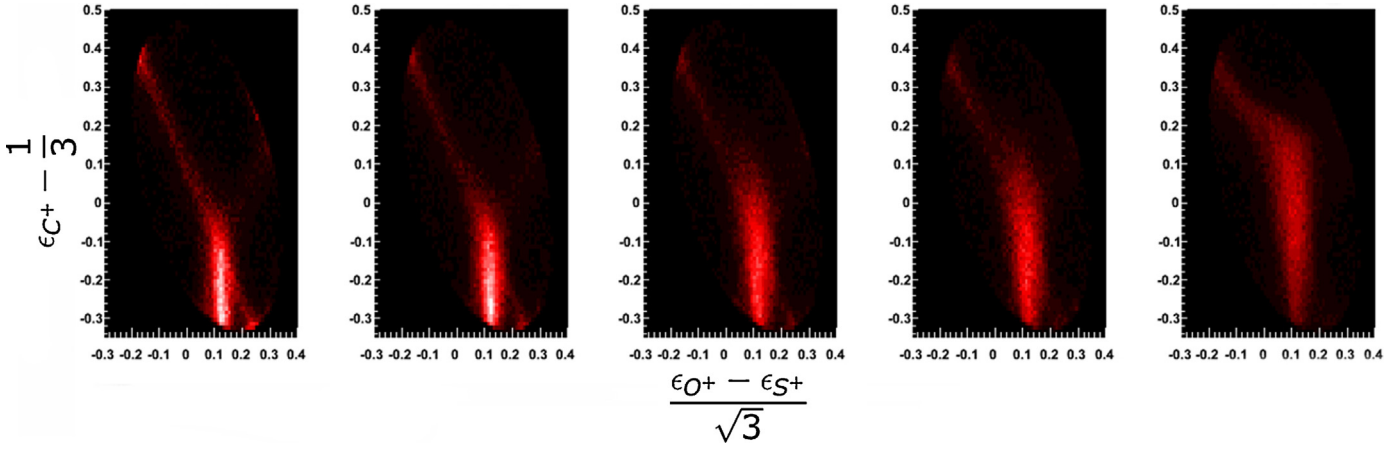


**Fig. 5.** Normalised Dalitz plots of (1,1,2) channel (left to right 7, 30, 60, 100 and 200 fs) showing the depletion of the stepwise channel (diagonal) with pulse length up to 60 fs and its re-emergence at higher pulse length.

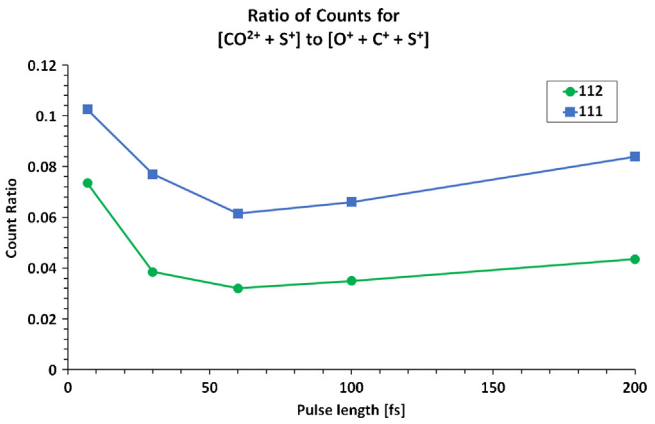


**Fig. 6.** Ratio of counts in the stepwise region to concerted processes region of Fig. 5 as a function of pulse length.

(1,1,2) channel where only two processes are allowed for clarity. As the pulse length is increased up to 60 fs, the diagonal signal representing the stepwise process fades, and then begins to become more prominent again for longer pulses. This process can be seen more explicitly in Fig. 6 which shows how the ratio of stepwise to concerted processes vary with pulse length. This surprising control mechanism can be understood within the framework of field induced bending and stretching [20]. Sato et al. showed that for $CO_2$, not only was bending initiated on the light dressed 2+ potential but that this was coupled with stretching, of the bonds. Their calculations indicated that the light induced potential pushes the molecule along the concerted coordinate stretching both bonds symmetrically, and giving the molecule momentum along the concerted break up coordinate. An important aspect of their calculation was that the timescale for this process was of tens of femtoseconds. We can understand the behaviour by thinking of the wave packet on the 3+ potential as a classical ball rolling on a two dimensional saddle point surface similar in form to that of the potential of Fig. 5 of [20]. As with $CO_2$ the 3+ potential has a local minimum followed by a maximum along the ($y = x$) diagonal (concerted bond expansion) and deep valleys along the $x$ and $y$ coordinates which correspond to stretching of the CO or CS bond only, with the CS being the deeper. Similarly for the 4+ state, the potential must have a valley along the CS stretch coordinate giving rise to the stepwise channel and this is likely accompanied by a shallow local minimum along the concerted coordinate. Evidence for this minimum from Fig. 1b is contained in observation that the peak energy released is only slightly lower for 30 fs than it is for 7 fs. For OCS we can see that for the shortest pulse length (sub 7 fs) the molecule passes through the intermediate channels quickly and the wave packet arrives on the 3+ and 4+ potential with little momentum. This lack of momentum along the concerted coordinate means some of the wave packet is directed down the favourable two body valleys in which only one of the bonds stretch. As the pulse length increases the impulse delivered on the 2+ potential increases because the molecule spends more time climbing the ionisation ladder and the wave packet arrives on the 3+ and 4+ states with momentum in the concerted coordinate direction allowing it to overcome any local maximum and diminishing the stepwise channel. With still further increase in pulse length however this concerted momentum is again reduced because the peak intensity of the laser decreases, now the wave packet again has a chance to slide down the valleys rather than overcome the saddle point maximum.

## 4. Conclusions

By using a compact representation offered by the Dalitz plot we can see, without attempting any complex molecular reconstruction process [31], how processes of molecular deformation and break up develop as pulse length is changed. Three stepwise channels have been identified, including one for the 4+ state. Furthermore, by careful control of laser pulse length, from few cycle to 200 fs, we can exert a degree of control over the final state molecular dissociation channel for the OCS molecule. The behaviour observed fits well into the picture predicted by [20] where the molecule is given momentum by the laser field, along the concerted bond breaking coordinate.

## References

[1] B.K. Yamanouchi, A. Hishikawa, A. Iwamae, Phys. Rev. Lett. 83 (1999) 1127–1130.
[2] J.H. Sanderson, W.A. Bryan, A. El-Zein, W.R. Newell, A.J. Langley, P.F. Taday, Phys. Rev. A 59 (1999) 2567–2570.
[3] J.H. Sanderson, W.A. Bryan, R.V. Thomas, W.R. Newell, I.D. Williams, A.J. Langley, P.F. Taday, J. Phys. B 31 (1998) 59–64.
[4] A. Hishikawa, A. Iwamae, K. Hoshina, M. Kono, K. Ymanouchi, Res. Chem. Intermed. 24 (1998) 765.
[5] H. Hasagawa, A. Hishikawa, K. Yamanouchi, Chem. Phys. Lett. 349 (2001) 57.
[6] A. Hishikawa, M. Ueyama, K. Yamanouchi, J. Chem. Phys. 122 (2005) 151104.
[7] M. Ueyama, H. Hasagawa, A. Hishikawa, K. Yamanouchi, Chem. Phys. 123 (2005) 154305.
[8] F. Légaré, K.F. Lee, I.V. Litvinyuk, P.W. Dooley, A.D. Bandrauk, D.M. Villeneuve, P.B. Corkum, Phys. Rev. A 72 (2005) 052717.
[9] F. Légaré, K.F. Lee, I.V. Litvinyuk, P.W. Dooley, S.S. Wesolowski, P.R. Bunker, P. Dombi, F. Krausz, A.D. Bandrauk, D.M. Villeneuve, P.B. Corkum, Phys. Rev. A 71 (2005) 013415.
[10] A. Hishikawa, E.J. Takahashi, A. Matsuda, Phys. Rev. Lett. 97 (2006) 243002.
[11] A. Hishikawa, A. Matsuda, M. Fushitani, E.J. Takahashi, Phys. Rev. Lett. 99 (2007) 258302.
[12] I. Bocharova, R. Karimi, E.F. Penka, J.P. Brichta, P. Lassonde, X. Fu, J.C. Kieffer, A.D. Bandrauk, I. Litvinyuk, J. Sanderson, F. Légaré, Phys. Rev. Lett. 107 (2011) 063201.
[13] R. Karimi, E. Bisson, B. Wales, S. Beaulieu, M. Giguère, Z.J. Long, W.K. Liu, J.C. Kieffer, F. Légaré, J. Sanderson, J. Chem. Phys. 138 (2013) 204311.
[14] D. Zeidler, A. Staudte, A.B. Bardon, D.M. Villeneuve, R. Dörner, P.B. Corkum, Phys. Rev. Lett. 95 (2005) 173201.
[15] E.A. Gibson, A. Paul, N. Wagner, R. Tobey, D. Gaudiosi, S. Backus, I.P. Christov, A. Aquila, E.M. Gullikson, D.T. Attwood, M.M. Murnane, H.C. Kapteyn, Science 302 (2003) 95.
[16] S. Haessler, J. Caillat, W. Boutu, C. Giovanetti-Teixeira, T. Ruchon, T. Auguste, Z. Diveki, P. Breger, A. Maquet, B. Carré, R. Taïeb, P. Salières, Nat. Phys. 6 (2010) 200.
[17] C. Vozzi, M. Negro, F. Calegari, G. Sansone, M. Nisoli, S. De Silvestri, S. Stagira, Nat. Phys. 7 (2011) 822.
[18] O. Smirnova, Y. Mairesse, S. Patchkovskii, N. Dudovich, D. Villeneuve, P. Corkum, M.Y. Ivanov, Nature 460 (2009) 972.
[19] T. Zuo, A.D. Bandrauk, Phys. Rev. A 52 (1995) R2511.
[20] Y. Sato, H. Kono, S. Koseki, Y. Fujimura, J. Am. Chem. Soc. 125 (2003) 8019.
[21] R.H. Dalitz, Phil. Mag. 44 (1953) 1068.
[22] W.A. Bryan, W.R. Newell, J.H. Sanderson, A.J. Langley, Phys. Rev. A 74 (2006) 053409.
[23] J.H. Sanderson, T.R.J. Goodworth, A. El-Zein, W.A. Bryan, W.R. Newell, A.J. Langley, P.F. Taday, Phys. Rev. A 65 (2002) 043403.
[24] B. Wales, T. Motojima, J. Matsumoto, Z.J. Long, W.K. Liu, H. Shiromaru, J. Sanderson, Phys. Scr. T156 (2013) 014068.
[25] B. Wales, T. Motojima, J. Matsumoto, Z.J. Long, W.K. Liu, H. Shiromaru, J. Sanderson, J. Phys. B 45 (2012) 045205.
[26] M.R. Jana, B. Ray, P.N. Ghosh, C.P. Safvan, J. Phys. B 43 (2010) 215207.
[27] B. Wales, E. Bisson, R. Karimi, J.C. Kieffer, F. Légaré, J. Sanderson, Nucl. Instrum. Methods Phys. Res. 667 (2012) 11.
[28] J.H.D. Eland, M. Hochlaf, P. Linusson, E. Andersson, L. Hedin, R. Feifel, J. Chem. Phys. 132 (2010) 014311.
[29] R. Karimi, B. Wales, E. Bissone, F. Legare, J. Kieffer, Sanderson, JPCS 388 (2012) 032049.
[30] N. Neumann, D. Hant, L.Ph.H. Schmidt, J. Titze, T. Jahnke, A. Czasch, M.S. Schöffler, K. Kreidi, O. Jagutzki, H. Schmidt-Böcking, R. Dörner, Phys. Rev. Lett. 104 (2010) 103201.
[31] J.P. Brichta, A.N. Seaman, J.H. Sanderson, Comput. Phys. Commun. 180 (2009) 197.